HYDROGEN, FUEL CELL & ENERGY STORAGE

Investigation of a fuel cell (FC) system for vehicle

Hadi Jafari | Hasan Hassanzadeh*

Department of Mechanical Engineering, University of Birjand, Birjand, Iran
* Corresponding author, Email: h.hassanzadeh@birjand.ac.ir

Article Information

Article Type
Research Article

Article History
Received: *09 Aug 2024*
Revised: *10 Oct 2024*
Accepted: *11 Oct 2024*
Published Online: *08 Nov 2024*

Keywords
PEM
Fuel cell
System
Vehicle

Abstract

The limited availability of fossil fuels, the technical challenges associated with existing vehicles, and their emissions, have made the study of efficient energy converters and clean fuels a top priority for research centers and automobile companies worldwide. Using a hybrid or non-hybrid FC system conventional vehicles can address some of their existing problems. Therefore, this study investigates a Polymer Electrolyte Membrane FC (PEMFC) system for vehicle applications. Modeling is performed using MATLAB software. According to the specifications of real-world samples, system components including stack, hydrogen and air humidifier, air compressor, humidifier pump, and cooling pump are modeled. The results indicate that 14% of the power generated by the FC stack is consumed by the peripheral components. In the basic state at a current density of $j = 0.7\,\mathrm{A/cm^2}$, the total efficiency of the system is 48.15%, while the net efficiency is 34.3%. By fully condensing the water vapor exiting the stack and using it to humidify the reactors, the need for an additional water tank is eliminated. For $j < 0.047\,\mathrm{A/cm^2}$, the stack cannot provide sufficient power for the system components, necessitating an auxiliary energy source, such as a battery, to start operation.

Cite this article: Jafari, H., Hassanzadeh, H. (2024). Investigation of a fuel cell (FC) system for vehicle. DOI: 10.22104/hfe.2024.6988.1307

 Publisher: Iranian Research Organization for Science and Technology (IROST)
DOI: 10.22104/hfe.2024.6988.1307

1 Introduction

Environmental pollution is a major global issue today, with transportation especially in large cities being a primary contributor. Currently, there are approximately 1.2 billion vehicles worldwide, with over 99% of them powered by Internal Combustion Engines (ICEs). The fuel of these vehicles is extracted from crude oil, which is considered ideal for vehicles due to its high-power density, ease of transportation and storage, and well-established infrastructure. Due to the low efficiency of ICEs and their operation at high temperatures, they emit harmful substances such as NO_x, CO, CO_2, HC, and particulate matter [1]. These issues have increased the focus on energy converters with higher efficiency, such as Fuel Cells (FCs), and the use of clean fuels like hydrogen.

Fuel Cells (FCs) directly convert the chemical energy of the fuel into electrical energy and are not constrained by the Carnot cycle [2]. Typically, FCs are categorized based on the type of electrolyte used. Among the various types of FCs, PEMFC is particularly suitable for transportation due to its high efficiency, high energy density, low operating temperature, and minimal noise, maintenance, and repair costs [3].

Figure 1 illustrates the components of PEMFC used in a FC stack, as well as the basic reactions occurring in the Catalyst Layers (CL).

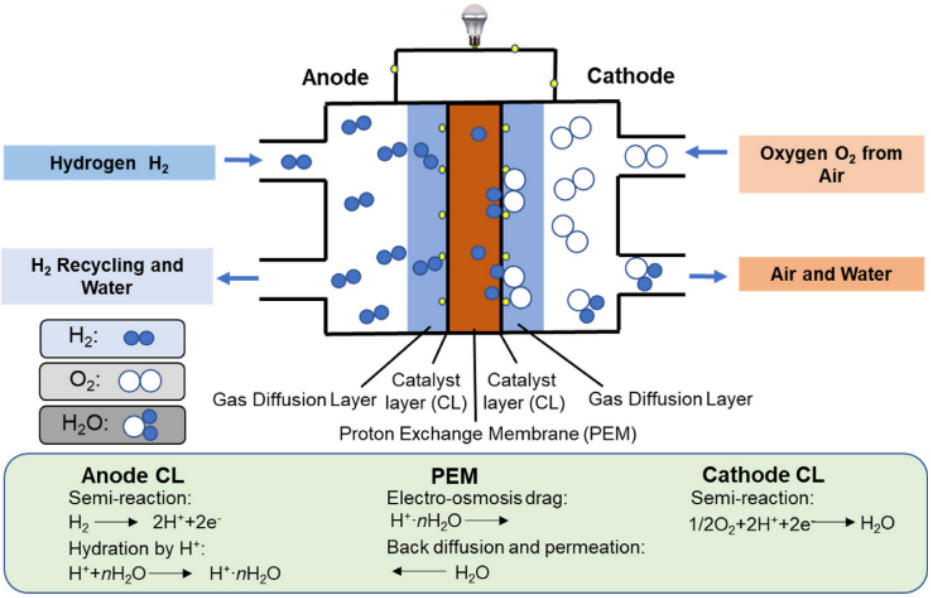

Fig. 1. Base reaction in PEMFC stack [4].

Figure 2 shows the efficiency curves for Carnot cycle, FC and a hybrid system combining the two [5]. According to this figure, at low temperatures the efficiency of ideal FCs exceeds that of HEs. As the temperature rises, the efficiency of FC decreases while the efficiency of HE increases. At approximately 800 °C, their ideal efficiencies become equal. However, a hybrid system that combines both an FC and an HE achieves a higher overall efficiency than either system alone.

Given the relative novelty of the FC vehicle compared to ICEs, extensive research is required to advance FC technology to the commercialization stage and enable it to compete effectively with ICEs. Currently, the high cost and low durability of Fuel Cells (FCs) are major obstacles to their competitiveness with Internal Combustion Engines (ICEs). Addressing these issues requires further research to improve both the affordability and longevity of FCs [2].

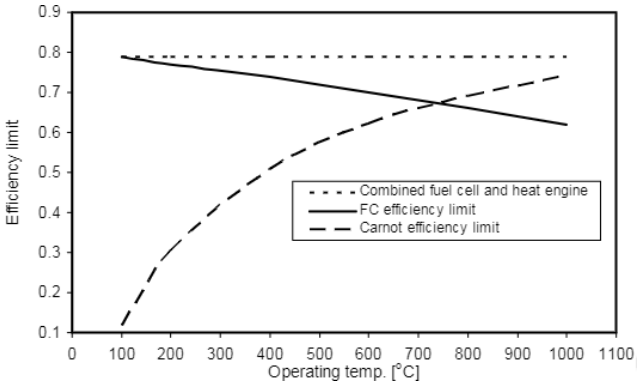

Fig. 2. Variations of ideal efficiency of FCs, HEs and hybrid systems vs. temperature [5].

The performance of FC vehicle on the road is complex due to the influence of several factors. Therefore, FC vehicle system performance can be broadly categorized into static and dynamic performance. During system start-up, steady-state operation, and shut-down, the performance of the Fuel Cell (FC) system is considered dynamic. In contrast, between these states, the system performance can be regarded as static. Extensive research has been conducted on both aspects, some of which are highlighted here. In 2001, Cownden et al. [6] presented a PEMFC system for transportation. They analyzed all system components, including the FC stack, compressor, hydrogen feeding section, and cooling section, from an exergy perspective. Their results show that the highest irreversibility occurs in the FC stack, followed by hydrogen ejector, air compressor, and cooling radiator of the FC stack. In 2006, Wishart et al. [7] presented and optimized a semiempirical model of a FC system with a power output of 1200 W, including axillary components. The optimization was based on two factors: maximum power and maximum exergy efficiency, and was applied to two contexts: transportation and power plants. In Iran, in 2008 Mirzaei and Masjidyan [8] designed and optimized a FC stack system for a motorcycle, including its auxiliary components in both hybrid and non-hybrid modes. Besides, in 2008, Pour Abedin and Omy [9] modeled a Fuel Cell (FC) hybrid vehicle and investigated factors affecting system performance, including control strategy, altitude, and road slope. In 2016, Hassanzadeh and Jafari [10] presented and optimized an FC system for vehicle applications and examined the impact of reactant moisture on the performance curve and output power.

Static models examine the operating conditions of a system at fixed points. However, to obtain the true response of a system to load changes, dynamic modeling is necessary. Even in static modeling, it is essential to use a dynamic model to analyze the start and end of the work cycle, as previously mentioned. The following sections will discuss several dynamic models. In 2005, Moore et al. [11] presented a dynamic model for a FC. This model includes four sub-systems: the FC stack, air feeding system, hydrogen feeding system, and water and heat management system. In 2008, Corbo [12] investigated a 20kW FC laboratory system under test cycles similar to those of car operation cycles. In 2016, Gharib and Hassanzadeh [13] presented a dynamic model to investigate the effect of inlet gas humidity on the dynamic response of a PEMFC stack. The results show that, firstly, the system's response to changes in current density is associated with a time delay. Secondly, as the relative humidity of the incoming gases increases, the ohmic voltage drop in the membrane decreases. The aim of this study is to develop a static model of a FC system for use in vehicles. Given the importance of humidification in polymer electrolyte membrane FC systems, this model places significant emphasis on the performance of the humidification system. In general, the key differences between this model and previous models are as follows:

- The model incorporates the characteristics of real components, including stacks, compressors, humidifiers, and pumps, to accurately represent the system's performance.
- The humidity levels of air and hydrogen are set according to the manufacturer's specifications.
- The appropriate compressor for this system is chosen based on the manufacturer's specifications.
- The thermal aspects of the FC system have been examined in more detail.

1.1 Introducing of vehicle system

Figure 3 presents a simple schematic of a fuel cell (FC) system used in a vehicle, along with its main components. As shown in the figure, the system is divided into four subsystems: the FC stack, the air supply subsystem (including the compressor, humidifier, and humidifier pump), the hydrogen supply subsystem (including the hydrogen storage tank, pressure regulation valve, and humidifier), and the cooling subsystem (consisting of the radiator, blower fan, water tank, and pump). After leaving the storage tank, the compressed hydrogen passes through the pressure regulation valve, and then it is heated and humidified before entering the FC. Similarly, the incoming air is compressed by the compressor, then cooled and humidified to the operating temperature and pressure of the FC before it enters the FC stack. In this system, the heat produced by compressing the air in the compressor can be used to heat hydrogen. If all the water vapor exiting the stack is in liquid form, this water can be used to humidify the incoming rea If all the water vapor exiting the stack is in liquid form, this water can be used to humidify the incoming reactants. The cooling system is responsible for dissipating the heat produced in the FC stack and maintaining a constant temperature.

2 Governing equations and system modeling

This section provides a detailed overview of the FC subsystems, including the FC stack, air and hydrogen supply, and cooling systems, and presents the governing equations for their modeling.

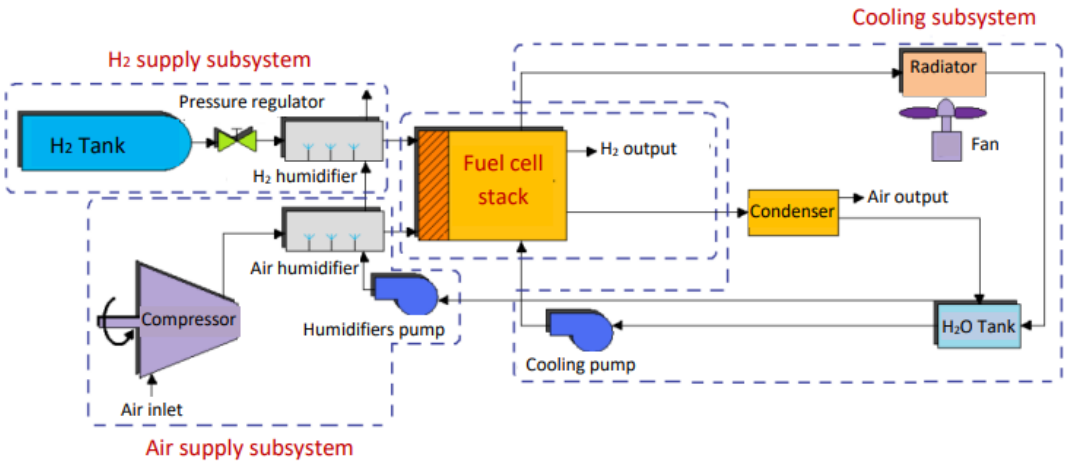

Fig. 3. A simple schematic of a vehicle FC system.

2.1 FC stack

Due to the complexity of the stack, analytical modeling is challenging; therefore, experimental and semi-experimental models are often employed to investigate its performance. In these models, the detailed processes inside the FC (such as electrochemical reactions) are less emphasized. Two examples are the models presented by Amfelt et al. [14] and Flower et al. [15], which investigated the activation potential loss and ohmic loss in PEMFCs. According to the Amfelt model, the activation voltage drop is expressed by the following polynomial:

$$\eta_{\text{act}} = \xi_1 + T_{\text{stack}}\left[\xi_2 + \xi_3 \ln(C^*_{\text{O}_2}) + \xi_4 \ln j\right]. \quad (1)$$

In this relation, j represents the current density, $C^*_{\text{O}_2}$ denotes the dissolved oxygen concentration in liquid water of the catalyst layer, and T_{stack} is the stack temperature. coefficients ξ depend on parameters such as Gibbs free energy, the cathode transfer coefficient and the concentrations of proton, hydrogen, oxygen and water concentrations, which are detailed in Table 1.

Table 1. Activation voltage loss coefficients [14,15].

ξ_i	Amphlett	Fowler
ξ_1	-0.951	-0.948
ξ_2	3.12×10^{-3}	[a]
ξ_3	7.40×10^{-5}	6.80×10^{-5}
ξ_4	-1.87×10^{-4}	-1.97×10^{-4}

[a] $\xi_2 = 0.00286 + 1.97 \times 10^{-4} \ln(A_{\text{act}}) + 4.30 \times 10^{-5} \ln(C^*_{\text{H}_2})$

Ohmic loss is calculated using Ohm's law, which accounts for the voltage drop resulting from the transfer of electrons in the electrodes and ions in the membrane, as expressed in Equation (2). The electrical resistance associated with electron transfer and contact resistance in the common section of the components can be neglected in comparison to the ionic resistance.

$$\eta_{\text{ohm}} = I(R_{\text{ele}} + R_{\text{ion}} + R_{\text{con}}). \quad (2)$$

In this relation I represents the current, R_{ele} is the ohmic resistance due to the transfer of electrons, and R_{ion} is the resistance of the membrane to the transfer of proton ions, which is calculated using the following equation:

$$R_{\text{ion}} = R_m \frac{t_m}{A_{\text{act}}}. \quad (3)$$

In this relation, t_m is the thickness of the membrane, A_{act} is the active surface of the electrode, and R_m is the specific resistance of the membrane. The specific resistance of the membrane is calculated using the following equation [7]:

$$R_m = \frac{181.6\left[1 + 0.03j + 0.062\left(\frac{T_{\text{st}}}{303}\right)^2 j^{2.5}\right] t_m}{(\lambda_{\text{mem}} - 0.634 - 3j)\exp\left[3.25\left(\frac{T_{\text{st}} - 303}{T_{\text{st}}}\right)\right]}. \quad (4)$$

In this relation, λ_{mem} represents the water content of the membrane, which is a function of the membrane's relative humidity.

The concentration loss is calculated using the following equation:

$$\eta_{\text{con}} = \frac{RT}{2F} \ln\left(\frac{j_L}{j_L - j}\right). \quad (5)$$

In this relation, j_L represents the limiting current density.

By calculating each of these losses and subtracting them from the reversible voltage of the FC, the net output voltage of cell is obtained.

$$V_{\text{cell}} = E_{\text{rev}} - (\eta_{\text{act}} + \eta_{\text{ohm}} + \eta_{\text{con}})\,. \tag{6}$$

In this relation, E_{rev} is the reversible voltage of FC, which is calculated using the Nernst equation. Assuming that all single cells in the FC stack have the same voltage at any current density, the voltage and output power of the FC stack, consisting of n single cells, are calculated as follows:

$$V_{\text{stack}} = nV_{\text{cell}}\,, \tag{7}$$

$$\dot{W}_{\text{stack}} = nV_{\text{cell}}\,I = V_{\text{stack}}\,I\,. \tag{8}$$

2.2 Air and hydrogen supply subsystems

The air supply system (including the compressor, humidifier, and humidifier pump) and the hydrogen supply system (including the hydrogen storage tank, pressure regulation valve, and humidifier) are responsible for providing the air and fuel required for the FC stack. These systems will be examined in detail below.

Compressor To use the advantages of working at high pressure, such as reducing the volume and weight of the FC stack, minimizing the size of pipes and connections, increasing the power density, and finally increasing the efficiency of the FC stack, a compressor is used to compress the incoming air. The compressor used in this model is the 1050OA-Autorotor [10] screw compressor, which is optimal in terms of efficiency and flexibility for pressures over 1.6 bar. The air compression ratio in the compressor depends on factors such as pressure drop in the cathodechannel and other system components, including the humidifier. The power consumption of the compressor, the output air temperature and the efficiency of the compressor are calculated using the following relations [7].

$$\dot{W}_{\text{comp}} = \dot{m}_{\text{air}} C_{p,\text{air}} \frac{T_{\text{air,in}}}{\eta_{\text{comp}}} \left[\left(\frac{P_{\text{cell}}}{P_{\text{air,in}}} \right)^{\frac{\gamma-1}{\gamma}} - 1 \right], \tag{9}$$

$$T_{\text{out}} = T_{\text{atm}} \left[1 + \frac{1}{\eta_{\text{comp}}} \left(\left(\frac{P_{\text{cell}}}{P_{\text{air,in}}} \right)^{\frac{\gamma-1}{\gamma}} - 1 \right) \right]. \tag{10}$$

In these relationships, $T_{\text{air,in}}$ represents the temperature of the air entering the compressor, and η_{comp} is the efficiency of the compressor, which is assigned a value of 60%.

Air and H_2 humidifiers The resistance of membrane to proton passage depends on its water content, so the membrane must always be kept hydrated. To ensure the membrane is fully hydrated and to reduce the resistance to proton passage, it is necessary to humidify both the fuel and oxidizer before they enter the FC stack. There are various types of humidifiers; in this research, membrane- type humidifiers are used. Due to their lack of moving parts and the absence of additional power requirements, these humidifiers are particularly advantageous in the FC system [16]. A humidifier is of the shell-and-tube type, with its schematic shown in Figure 4. The tubes in the humidifier are made of Nafion, with air (or H_2) flowing through the tubes and water circulating around the shell. Due to the partial pressure difference across the membrane, water vapor is transferred through the membrane and added to the airflow [17]. The specifications of the humidifiers used in the air and hydrogen supply subsystem are provided in Table 2 [18].

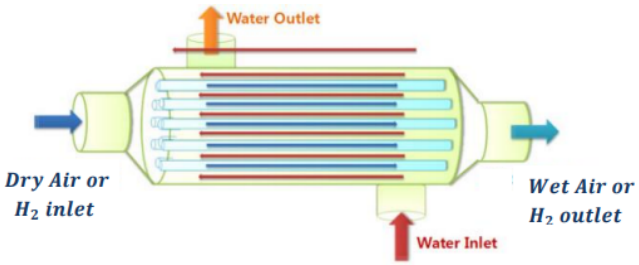

Fig. 4. Schematic of air (fuel) membrane humidifier, shell-tube type [16].

Table 2. Specifications of Perma Pure membrane humidifiers for Air and H_2.

Geometric characteristics of humidifiers	Air, model: FC600-7000	H_2, model: FC300-1660-7Lp
$d_{\text{in,pipe}}$ (mm)	0.76	1.02
$d_{\text{out,pipe}}$ (mm)	0.71	0.97
L_{pipe} (mm)	177.8	177.8
$d_{\text{in,shell}}$ (mm)	154	280.88
n_{pipe}	7000	240

In the humidifier model, it is possible to calculate the water consumption rate, heat transfer rate, and pressure drop in both the shell and pipe. The relative humidity of the air along the pipe can be calculated using the following equation [19]:

$$\text{RH}_{\text{air}} = 1 - (1 - \text{RH}_{\text{air,in}}) \exp\left(-\frac{2k_w R T_{\text{wv}} z}{v r_i} \right). \tag{11}$$

In this equation, T_{wv} represents the temperature of water vapor, z is the distance from the beginning of the pipe and k_w is an experimental parameter that depends on the membrane thickness. The parameter values for different kinds of membranes are provided in Table 3.

Table 3. The value of k_w for different kinds of membrane [17].

Nafion type	t_m (μm)	k_w (kg/m$^2 \cdot$ s $\cdot$ atm)
111	25	20×10^{-5}
112	50	8.9×10^{-5}
1135	87	6.7×10^{-5}
115	125	5.3×10^{-5}
117	175	2.3×10^{-5}

The water consumption of the humidifier is calculated as follows:

$$\dot{m}_{\mathrm{H_2O}} = \mathrm{RH}_{\mathrm{air}} \times 0.622\, P_{\mathrm{H_2O,sat}} \times \left(\frac{\dot{m}_{\mathrm{air,dry}}}{P_{\mathrm{air,dry}}}\right) \quad (12)$$

Since the amount of water vapor added to the air passing through the humidifier shell is relatively small compared to the volume of air, the fluid flow in this type of humidifier is similar to that in a shell-tube heat exchanger. Therefore, the methods used in shell-and-tube heat exchangers have been applied to calculate the heat transfer rate, outlet temperatures, and pressure drop. Specifically, the ε-NTU method is employed to calculate heat exchange and outlet temperatures, given that the input temperatures of both air and water are known [10].

To calculate the pressure drops in the humidifier shell, the humidifier is divided into three sections: the inlet and outlet nozzles, the initial and final areas, and the intermediate regions [20]. The relations used to determine the pressure drop in the shell are provided in Table 4.

Table 4. Pressure drops relations in the humidifier shell [20].

Region	Pressure Loss relation
Inlet and outlet nozzles	$\Delta p_1 = \rho_w u_n^2$
Entrance and exit region	$\delta p_2 = \rho_w f u_n^2 N_c f_b f_c (\mu_{\mathrm{sw}}/\mu_s)^{0.14}$
Middle region	$\Delta p_3 = f L \rho_w u_n^2 / D_h$

By calculating the pressure drop in the humidifier shell, the power consumption of the humidifier pump can be determined using the following equation.

$$\dot{W}_{\mathrm{pump}} = \frac{\dot{m}_{\mathrm{H_2O}} \Delta P_{\mathrm{loss}}}{\rho \eta_{\mathrm{pump}} \eta_{\mathrm{motor}}}\,. \quad (13)$$

In this calculation, the efficiency of the pump is assumed to be 60%, and the efficiency of the electric motor is 80%. Additionally, the pressure of the hydrogen storage tank remains constant during operation. The hydrogen humidifier system is similar to the air humidifier system, but due to the lower flow rate of hydrogen compared to air, its dimensions are smaller.

2.3 Cooling subsystem

The performance of the FC stack is highly dependent on temperature; excessive temperatures can damage the membrane, making it crucial to maintain the FC at its operating temperature of 80 °C. The amount of heat generated in the FC stack, as well as the water flow and power required for heat removal, are calculated using Equation (13):

$$\dot{Q} = nI(1.48 - V_{\mathrm{cell}})\,, \quad (14)$$

$$\dot{m}_{\mathrm{cool,H_2O}} = \frac{\dot{Q}_{\mathrm{net}}}{c_{p,\mathrm{H_2O}}(T_{\mathrm{stack}} - T_{\mathrm{cool,H_2O,in}})}\,. \quad (15)$$

In this context, 1.48 V represents the theoretical voltage achieved if all the chemical energy of the fuel and oxidizer is converted into electricity and the produced water is released as liquid. Approximately 20% of the heat generated in the FC is removed by the fuel and oxidizer flows in the channels, meaning that about 80% of the heat produced in the FC is removed through the cooling system. Thus, $\dot{Q}_{\mathrm{net}} \approx 0.8\,\dot{Q}_{\mathrm{stack}}$.

2.4 Solution and validation

In the previous section, the components of the FC system were introduced. This section discusses the modeling of the FC system. A schematic of the model of this system is shown in Figure 5. This system includes four subsystems: the hydrogen supply subsystem, the air supply subsystem, the FC stack, and the cooling subsystem. The system input comprises current density j, air and H_2 stoichiometries ($\mathrm{Sto_{air\&H_2}}$), the FC stack temperature, air inlet temperature, and the anode and cathode pressures. The system can produce several outputs, including net and gross power, compressor power consumption, water consumption, stack voltage, heat generated, and both stack and overall system efficiency.

The simulation model for the FC vehicle behavior has been developed using MATLAB Simulink. The model created for the system and its components is illustrated in Figure 6.

The working conditions of the system in this model are given in Table 5. To validate the model's accuracy, Figure 7 presents the output power of the stack and the net power of the modeled system for a 1.2 kW FC stack, as referenced in [7]. The average results show a 3.8% deviation from Wishart's findings.

In Figure 8, the rate of water consumption in the humidifier in the current model is compared with reference [16]. The results show a good trend and the average error is 6.7%.

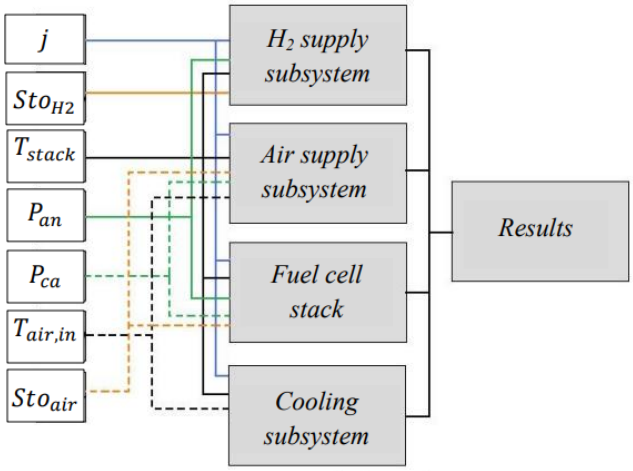

Table 5. Basic input values for system modeling.

ST_{air}	ST_{H_2}	P_{ca}	P_{an}	T_{atm}	T_{stack}
2.5	1.1	3 atm	3 atm	298 K	355 K

Fig. 5. Simple schematic of FC system model.

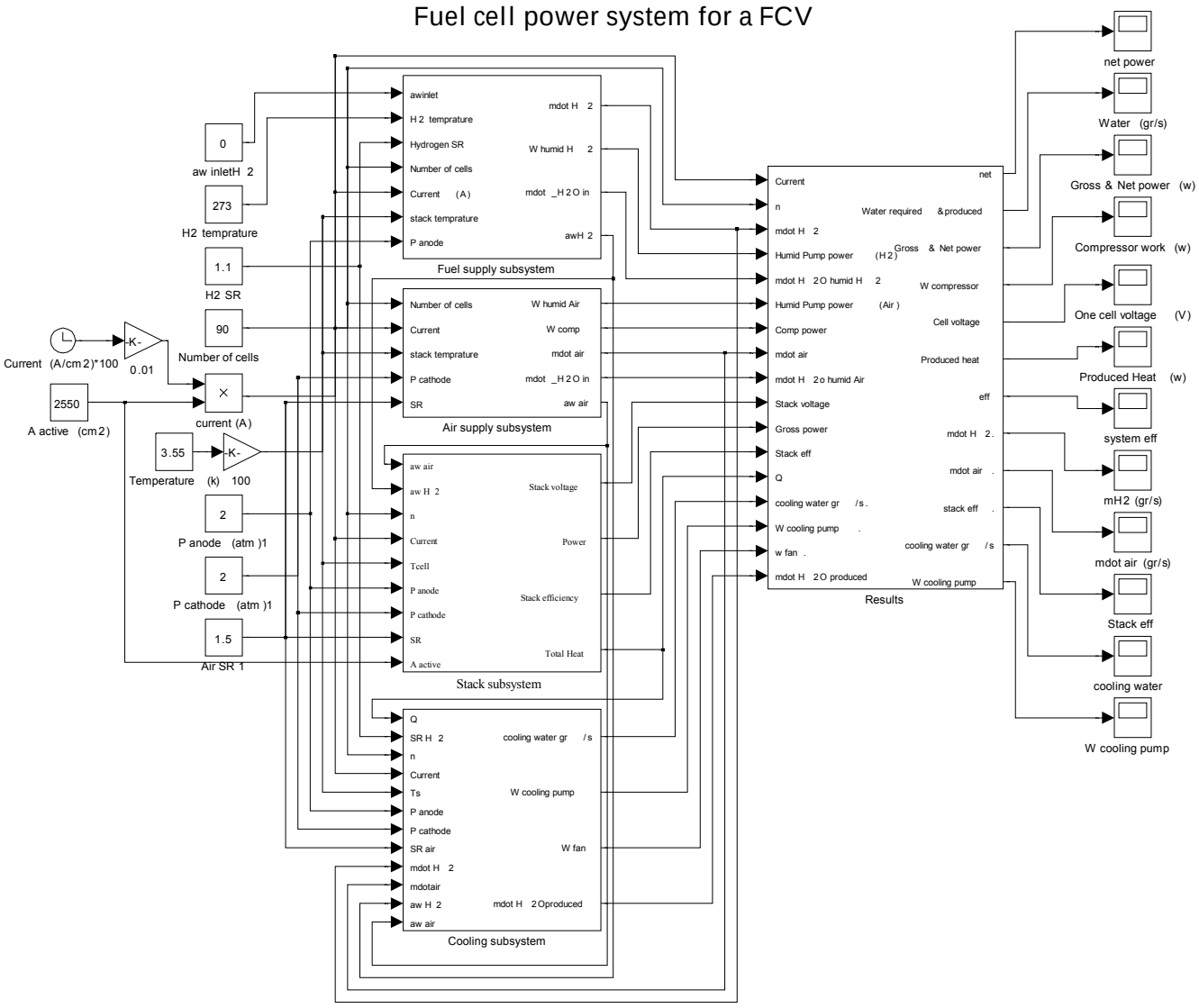

Fig. 6. Fuel cell power system model for an FCV.

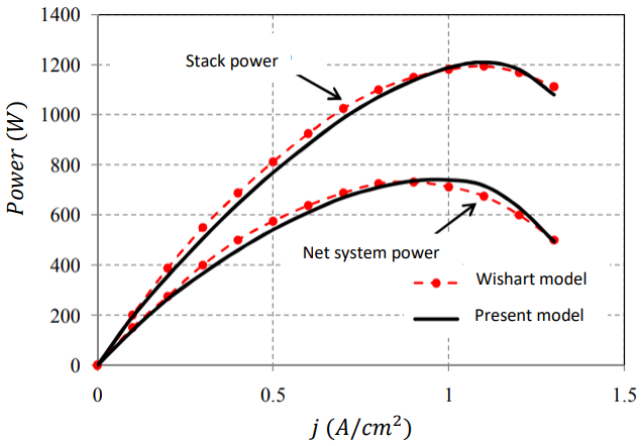

Fig. 7. Comparison of the stack output power and the net system power with Wishart results [7].

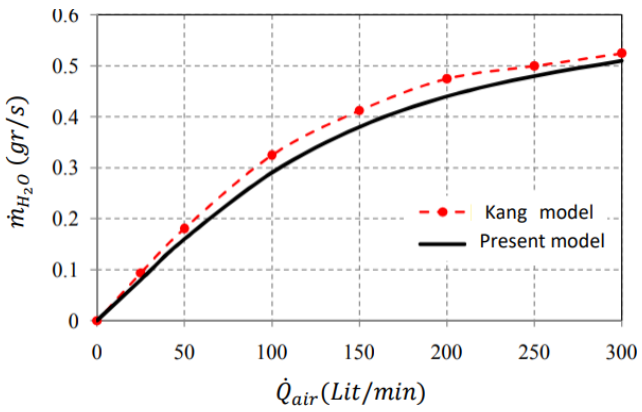

Fig. 8. Water consumption rate of Perma Pure 150-480-7PP shell-tube membrane humidifier and its comparison with Kang's results [16].

3 Results and Discussion

The modeling results are presented in Figures 9 to 16. Figures 9 and 10 illustrate the effects of temperature and pressure on the performance curve of the PEMFC used in the stack. While increasing the temperature decreases the reversible voltage, which is undesirable, it also enhances the reaction kinetics at the electrodes, which is beneficial. Increasing the kinetics of the electrode reactions reduces activation losses and ultimately enhances the efficiency of the FC. However, the temperature limitations of the membrane prevent the temperature from rising excessively increasing the pressure does not significantly affect on the reversible voltage; however, it increases the concentration of reactants in the electrodes, thereby enhancing the rate of electrochemical reactions. As shown in Figure 10, this leads to a moderate improvement in the performance curve of the FC. Increasing pressure is particularly important in the miniaturization of FC systems, although it complicates the sealing of these systems. In FC systems, however, higher pressure leads to increased power consumption by the compressor. Therefore, it is crucial to calculate the optimal pressure that maximizes the net power of the system, balancing the increased power consumption of the compressor with the power output of the FC stack.

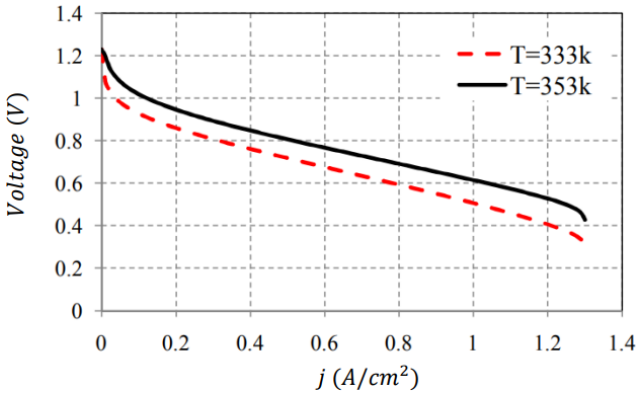

Fig. 9. The effect of operating temperature on FC performance.

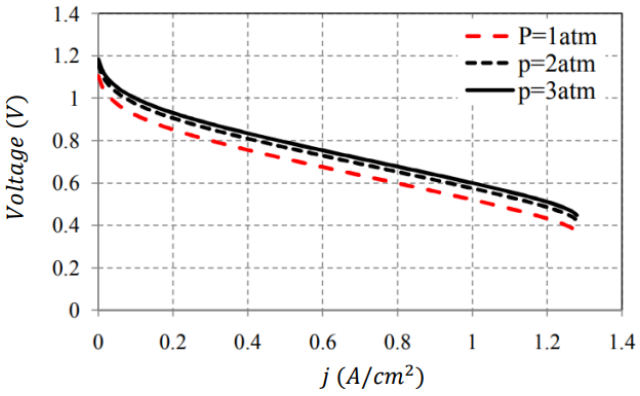

Fig. 10. The effect of operating pressure on FC performance

In Figure 11, the curves representing the changes in air and hydrogen consumption flow rates are plotted against current density. Firstly, the flow rates of both air and hydrogen consumption are directly proportional to the current density. Secondly, due to the low concentration of oxygen in the air, along with the lower stoichiometric coefficient and molecular mass of hydrogen compared to air, the flow rate of air entering the FC stack is significantly higher than that of hydrogen.

In Figure 12, the performance curve of a single cell, along with the output power of the FC stack and the net power of the system is presented. For the system stack with a maximum power of 50 kW, the maximum

output power of the system is 30 kW, which occurs at a current density of 1 A/cm^2. At the current densities below 0.047 A/cm^2, the FC stack is unable to supply the power needed for the system components, necessitating an auxiliary power source, such as a battery, during start-up.

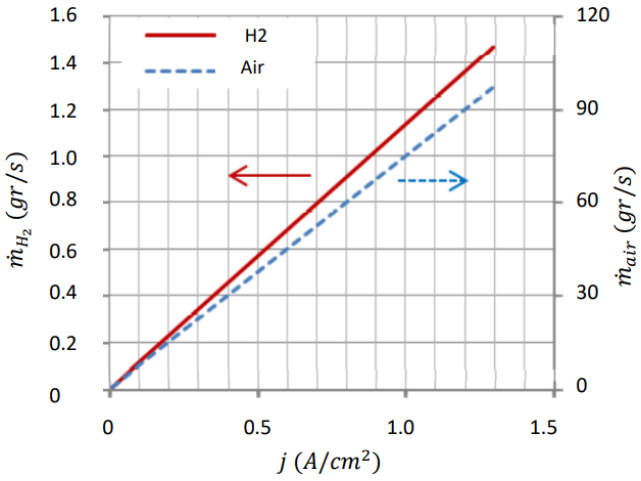

Fig. 11. Air and H_2 mass consumption rate of FC stack.

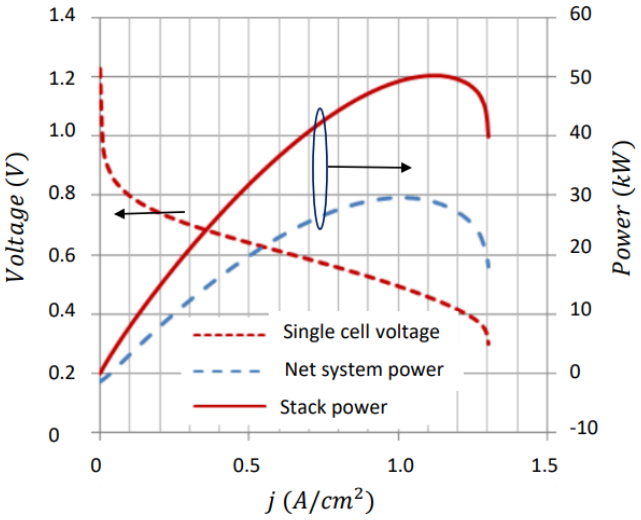

Fig. 12. The performance of a single FC, the output stack power and the system net power.

Figure 13 illustrates the curve showing the pressure loss of water flow through the air humidifier shell as a function of current density for three different values of inlet air relative humidity. As observed, with an increase in the relative humidity of the inlet air, the pressure loss in the shell decreases. This is because the required flow of water to humidify the air in the shell is reduced, ultimately leading to a decrease in the power demand of the humidifier's pump.

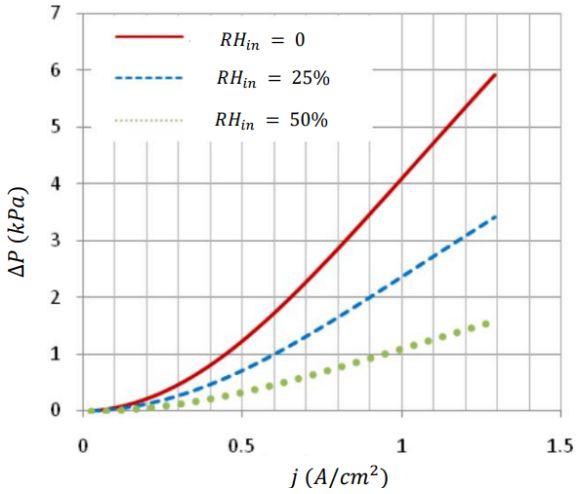

Fig. 13. Pressure drop in the shell of air humidifier.

Figure 14 shows the curves for the rate of water consumed by the humidifiers, the water produced by the FC stack and the water exiting the stack, all plotted against current density. The water produced in the FC and, consequently, in the FC stack is proportional to the current density, as described by the equation $\dot{m}_{\mathrm{H_2O}} = M\frac{j}{2F}$. Thus, the water production curve in the stack increases linearly with increasing current density. However, the flow rate of water required for humidifying the fuel and oxidizer depends on additional parameters beyond just the current density. The water output from the FC stack is equal to the sum of the water produced in the stack and the water needed for humidifying the fuel and oxidizer. The figure indicates that if the water exiting the FC stack is liquefied, the system will not require additional water for humidification after the initial start-up phase.

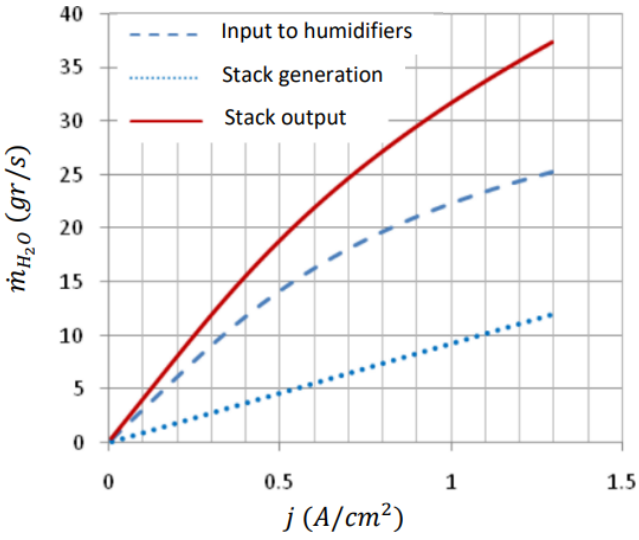

Fig. 14. Rate of water necessary for humidifiers, produced water and water output from the stack.

Figure 15 illustrates the efficiency of the FC stack as a function of current density. The efficiency of the FC stack is defined as the ratio of the stack's power output to the enthalpy of H_2/O_2 Reaction. If all the energy released in this reaction is converted into electricity, the corresponding voltage is termed the hypothetical voltage, which is calculated as $E_H = |\delta\hat{h}|/nF = 1.48\,\mathrm{V}$ [21]. Therefore, the efficiency of a FC stack can be defined as the ratio of the output voltage to 1.48 or $\eta_{\mathrm{stack}} = V/1.48$. Since the efficiency of a FC is proportional to its output voltage, the efficiency curve is similar to the performance curve of a FC. As current density increases, irreversibility also increase, leading to a decrease in stack efficiency. The influence of operating parameters, such as temperature and pressure, on this efficiency curve is similar to their effect on the output voltage of the FC.

Figure 16 displays the efficiency of the FC system. The maximum efficiency is observed at low current densities. As current density increases, the rate of air required also rises, leading to higher power consumption for air compression, which reduces overall system efficiency. However, operating at a current density of $0.16\,\mathrm{A/cm^2}$ increases the size and cost of the FC. While this increase in size may be manageable for power generation stations and stationary combined heat and power (CHP) systems, it poses a significant issue for vehicles. For an FC vehicle, it is essential to operate at an average current density within approximately 50% of the maximum power of the FC stack.

4 Conclusions

In this study, a FC system designed for vehicle use has been examined. The system includes an FC stack, air and hydrogen feeding subsystems, and cooling subsystems. The analysis was conducted using the Simulink environment in MATLAB, and the results were validated against data from existing literature. The results indicate that the FC stack achieves its highest net output power at a current density of approximately $1\,\mathrm{A/cm^2}$.

Additionally, as the relative humidity of the air entering the humidifier increases, the pressure drops across its shell decreases, which in turn reduces the power consumption of the pump. When the water vapor exiting the FC stack is fully condensed, the water required for the humidifier can be adequately supplied, except during the initial start-up phase. Among the various components, the compressor consumes the most power, while the humidifier pump consumes the least. For instance, in the baseline condition at a current density of $0.7\,\mathrm{A/cm^2}$, the compressor uses 13.8% of the stack's production power, whereas less than 1% of the production power is consumed by the cooling pump and the humidifier pump.

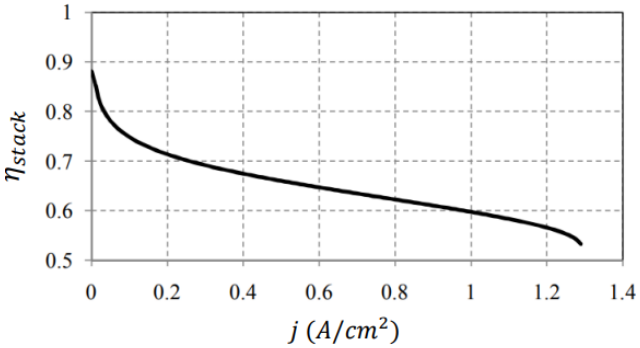

Fig. 15. Stack efficiency.

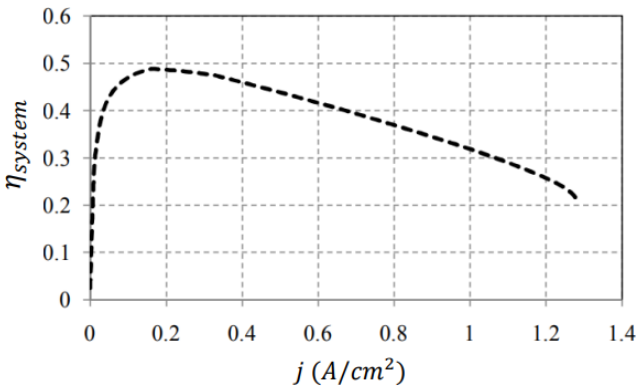

Fig. 16. The total efficiency of FC system.

References

[1] Singh S, Ganeshwar R D, Dixit M. Future of Transportation- A Comparison between Internal Combustion Engine, Electric Vehicles and Fuel Cell Vehicles. Universal Journal of Mechanical Engineering. 2023;11:13–23. 260

[2] Hassanzadeh H, Mansouri S. Efficiency of ideal fuel cell and carnot cycle from a fundamental perspective. Proceedings of the Institution of Mechanical Engineers, Part A: Journal of Power and Energy. 2005;219(4):245–254. 260

[3] Wang J. System integration, durability and reliability of fuel cells: Challenges and solutions. Applied Energy. 2017;189:460–479. Available from: https://www.sciencedirect.com/science/article/pii/S0306261916318530. 260

[4] Wang Y, Yang X, Sun Z, Chen Z. A systematic review of system modeling and control strategy of proton exchange membrane fuel cell. Energy Reviews. 2023;p. 100054. 260

[5] Welaya YM, Mosleh M, Ammar NR. Thermodynamic analysis of a combined gas turbine power plant with a solid oxide fuel cell for marine applications. International Journal of Naval Architecture and Ocean Engineering. 2013;5(4):529–545. 260

[6] Cownden R, Nahon M, Rosen MA. Exergy analysis of a fuel cell power system for transportation applications. Exergy, An International Journal. 2001;1(2):112–121. 261

[7] Wishart J, Dong Z, Secanell M. Optimization of a PEM fuel cell system based on empirical data and a generalized electrochemical semi-empirical model. Journal of Power Sources. 2006;161(2):1041–1055. Available from: https://www.sciencedirect.com/science/article/pii/S0378775306012250. 261, 262, 263, 264, 266

[8] Mirzai M, Masjidyan MH. Design and simulation of a hybrid FC motorcycle and its comparison with non-hybrid system. In: The first national hydrogen and FC conference. Tehran; 2017. In Persian. 261

[9] Pourabdin G, Amy F. How a FC hybrid vehicle performs in different working and environmental conditions. In: The first national hydrogen and FC conference. Tehran; 2017. In Persian. 261

[10] Hassanzadeh H, Jafari H. Modeling and optimization of FC vehicle driver system with power of 50kW. Modares Mechanical Engineering. 2016;16:141–152. In Persian. Available from: https://mme.modares.ac.ir/article-15-3376-en.html. 261, 263, 264

[11] Moore R, Hauer K, Friedman D, Cunningham J, Badrinarayanan P, Ramaswamy S, et al. A dynamic simulation tool for hydrogen fuel cell vehicles. Journal of Power Sources. 2005;141(2):272–285. 261

[12] Corbo P, Migliardini F, Veneri O. Experimental analysis of a 20ákWe PEM fuel cell system in dynamic conditions representative of automotive applications. Energy Conversion and Management. 2008;49(10):2688–2697. 261

[13] Gharib S, Hassanzadeh H. Investigation of the effect of humidification of inlet gases on the dynamic response of a PEM FC stack. Modares Mechanical Engineering. 2017;17:433–443. In Persian. Available from: https://mme.modares.ac.ir/browse.php?a_id=2611&sid=15&slc_lang=en. 261

[14] Amphlett JC, Baumert RM, Mann RF, Peppley BA, Roberge PR, Harris TJ. Performance modeling of the Ballard Mark IV solid polymer electrolyte fuel cell: I. Mechanistic model development. Journal of the Electrochemical Society. 1995;142(1):1. 262

[15] Fowler MW, Mann RF, Amphlett JC, Peppley BA, Roberge PR. Incorporation of voltage degradation into a generalised steady state electrochemical model for a PEM fuel cell. Journal of power sources. 2002;106(1-2):274–283. 262

[16] Kang S, Min K, Yu S. Two dimensional dynamic modeling of a shell-and-tube water-to-gas membrane humidifier for proton exchange membrane fuel cell. International journal of hydrogen energy. 2010;35(4):1727–1741. 263, 264, 266

[17] Park S, Oh IH. An analytical model of Nafion™ membrane humidifier for proton exchange membrane fuel cells. Journal of Power Sources. 2009;188(2):498–501. 263, 264

[18] http://www.permapure.com;. 263

[19] Kapale UC, Chand S. Modeling for shell-side pressure drop for liquid flow in shell-and-tube heat ex-

changer. International Journal of Heat and Mass Transfer. 2006;49(3-4):601–610. 263

[20] Jafari H. Modeling and optimization of a polymer FC system with a power of 50 kW for use in transportation; University of Birjand. 264

[21] O'hayre R, Cha SW, Colella W, Prinz FB. Fuel cell fundamentals. John Wiley & Sons; 2016. 268